

# Fluorination of Mxene by Elemental F<sub>2</sub> as Electrode Material for Lithium-Ion Batteries

Bishnu P. Thapaliya,<sup>[a]</sup> Charl J. Jaftha,<sup>\*[b]</sup> Hailong Lyu,<sup>[b]</sup> Jiexiang Xia,<sup>[b]</sup> Harry M. Meyer III,<sup>[c]</sup> M. Parans Paranthaman,<sup>[b]</sup> Xiao-Guang Sun,<sup>[b]</sup> Craig A. Bridges,<sup>[b]</sup> and Sheng Dai<sup>\*[a, b]</sup>

The transformation of MXene sheets into TiOF<sub>2</sub> 2D sheets with superior electrochemical performance was developed. MXene synthesized from Ti<sub>3</sub>AlC<sub>2</sub> was fluorinated for 3-, 6-, and 24 hours, respectively, by means of a direct fluorination process. Exposure of MXene powder to elemental fluorine for 3 hours induced the formation of CF<sub>2</sub> groups and TiF<sub>3</sub> on the surface, which have beneficial effects on the electrochemical performance. X-ray photoelectron spectroscopy suggested that after fluorinating the MXene sample for 6 hours, Ti<sup>2+</sup> and Ti<sup>3+</sup> were not present on the surface but only Ti<sup>4+</sup>, indicating the formation of TiOF<sub>2</sub>. XRD indicated that TiOF<sub>2</sub> was present after fluorinating for 3 hours, and after 24 hours the MXene had transformed to TiOF<sub>2</sub> with minor impurities remaining, maintaining its 2D layer morphology. The 24 hours fluorinated sample with its TiOF<sub>2</sub> phase showed superior capacity that increased with cycle number. It also had a better rate capability than non-2D-layered TiOF<sub>2</sub>, indicating the advantage of the 2D-layered morphology derived from the parent MXene phase.

## Introduction

In the pursuit to engineer better electrode materials for lithium ion batteries (LIBs), Ti<sub>3</sub>AlC<sub>2</sub> that is part of the MAX phases, was shown to form 2D Ti<sub>3</sub>C<sub>2</sub> crystals (MXene) through selective HF etching of the Al layers<sup>1</sup>. Additionally, it was also shown that MXene can be produced using safer handling HF-containing (NaF<sub>2</sub>, KHF<sub>2</sub> and NH<sub>4</sub>HF<sub>2</sub>)<sup>2</sup> and HF-forming (LiF + HCl)<sup>3</sup> etchants. Regardless of which method is used to prepare MXene, the etching results in surface F and OH surface functional groups due to the presence of HF and water. Given the presence of 2D layers, MXene has been widely studied for its electrochemical applications and specifically for LIBs as an intercalation pseudocapacitor electrode<sup>4-10</sup>. However, due to the compact atomic

arrangement of MXene, that would hinder the diffusion of Li<sup>+</sup> perpendicular to the layer plane, the electrodes have a reduced power density<sup>11</sup>. In order to increase the power density of MXenes, Ma et al.<sup>12</sup>, for example, prepared hybrid 3D porous MXene / reduced graphene oxide films where the 3D structure facilitates the diffusion of Li<sup>+</sup>. Another possibility to enhance the electrochemical performance of MXene electrodes is by changing their surface functional groups – calculations have shown that MXenes have a tunable band gap controllable by changing their surface termination<sup>1,13</sup>. It was also demonstrated that post-etch annealing of MXenes in different gas environments resulted in changes in the surface termination, structure and thus their electrochemical performance<sup>14</sup>. It is therefore clear that the exploration of other fluorination methods of MXenes would result in different surface termination products that would influence their electrochemical properties.

Currently, conversion electrodes are investigated as alternatives to traditional intercalation electrode materials to enhance the energy density of LIBs. Conversion electrodes have shown promise for the development of high reversible capacities. Within this class of electrodes several oxyfluorides have attracted interest, and it is important to note that these may display intercalation behavior early in the discharge cycle. These include transition metal oxyfluorides such as FeOF, NbO<sub>2</sub>F and TiOF<sub>2</sub> that are typically synthesized by solid state reactions and wet chemistry. Of these examples, TiOF<sub>2</sub> has been synthesized by multiple methods, including: i. immersion of anatase TiO<sub>2</sub> in an HF solution for 24 hours, followed by evaporation, or evaporation and calcination in an Ar atmosphere at 400 °C<sup>15,16</sup>; ii. direct fluorination of TiO<sub>2</sub> to form TiOF<sub>2</sub><sup>17</sup>. TiOF<sub>2</sub> offers advantages from both the oxide and fluoride anions for improved capacity, high voltage, good conductivity and stable charge/discharge cyclability<sup>18</sup>.

Fluorination has drawn attention as a tool for post-processing in order to modify materials for enhanced properties in different applications<sup>17,19-23</sup>. There are several methods of fluorinating materials, such as the wet chemical method in which the material is dispersed and reacted with a fluorinated solution (i.e. HF, NH<sub>4</sub>HF<sub>2</sub>, etc.), which in the case of Ti<sub>3</sub>AlC<sub>2</sub> is also ideal for causing exfoliation through preferential etching of Al from the structure; in this approach the F content is low and thus the yield is limited<sup>24,25</sup>. Other approaches include low temperature solid state reaction with fluorinating agents such as NH<sub>4</sub>F, CuF<sub>2</sub>, ZnF<sub>2</sub>, PVDF or XeF<sub>2</sub>, electrochemical fluorination, or direct fluorination in plasma (e.g., CF<sub>4</sub> and SF<sub>6</sub> fluorine sources); these reagents may be expensive (e.g., XeF<sub>2</sub>), and may require relatively high temperatures (~350 °C) for fluorination<sup>19,24</sup>. Where lower temperatures are required to stabilize a reaction product, the more aggressive direct fluorination with F<sub>2</sub> may be used<sup>20,22,23</sup>. The fluorination method used must therefore be tailored to the reaction product of interest,

[a] Mr. B.P. Thapaliya, Prof. S. Dai  
Chemistry Department  
University of Tennessee, Knoxville, Tennessee 7996, United States  
E-mail: dais@ornl.gov

[b] Dr. C.J. Jaftha, Dr. H. Lyu, Dr. J. Xia, Dr. M.P. Paranthaman, Dr. X-G. Sun, Dr. C.A. Bridges, Dr. S. Dai  
Chemical Science Division  
Oak Ridge National Laboratory, Oak Ridge, Tennessee 37831, United States  
E-mail: jafthacj@ornl.gov

[c] Dr. H.M. Meyer III  
Chemical Science Division  
Oak Ridge National Laboratory, Oak Ridge, Tennessee 37831, United States

along with careful control of experimental conditions. A direct fluorination method was thus developed by the Dai group<sup>26</sup> where different materials can be fluorinated at relatively low temperatures for enhanced properties.

In this work we demonstrate that direct fluorination of MXene can produce a high degree of fluorination with retention of overall 2D sheet-like particle morphology. The fluorinating time results in different F species on the surface of the material that have electrochemical implications. By increasing the fluorination time to 24 hours, the MXene based phase is fully converted to TiOF<sub>2</sub> with superior electrochemical performance in terms of increased capacity, rate capability and cycling stability.

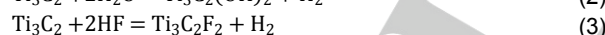
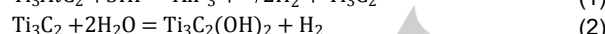
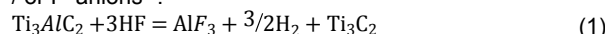
## Results and Discussion

Fluorination with elemental F<sub>2</sub> of the HF treated powders resulted in a significant weight gain, with an apparent increase in surface area, as indicated in **Table 1**. The weight gain of recovered powders suggests a high degree of oxidation (through fluorination) of the precursor powders. To understand this oxidation, it is necessary to consider the possible reaction pathways provided by the precursor powder.

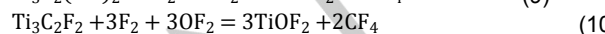
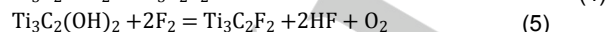
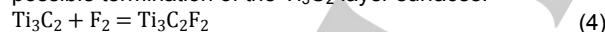
**Table 1.** Experimental conditions for the fluorination process, weight increase after fluorination and the BET surface areas of the samples.

Sample	Fluorination Time [hours]	F <sub>2</sub> Flow rate [SCCM]	weight gain [%]	BET Surface Area [m <sup>2</sup> /g]	Fluorination temperature [°C]
MXene	0	-	-	9.1 ± 0.1	≤ 150
FMX3	3	1.8	8.3	9.4 ± 0.1	
FMX6	6	1.8	43.1	11.6 ± 0.2	
FMX24	24	1.8	85.9	14.2 ± 0.2	

The Ti<sub>3</sub>C<sub>2</sub> may react further with species in solution after removal of Al, resulting in termination of Ti<sub>3</sub>C<sub>2</sub> layer surfaces with OH<sup>-</sup> and / or F<sup>-</sup> anions<sup>1</sup>:



Upon fluorination with F<sub>2</sub>, several reaction mechanisms may be considered based upon known fluorinated compounds and possible termination of the Ti<sub>3</sub>C<sub>2</sub> layer surfaces:



These possible reaction pathways can account for the formation of different species during the different reaction times, though alternate mechanisms with loss of TiF<sub>4</sub> through sublimation are not considered as the extent of this is difficult to verify. The largest weight gain of these would be the overall reaction of Ti<sub>3</sub>C<sub>2</sub> to form TiOF<sub>2</sub>, but given that it is expected for OH<sup>-</sup> or F<sup>-</sup> anions to be present after the HF treatment; to account for the weight gain it is necessary to consider whether other oxidized species are

present, such as partially fluorinated carbon that has not escaped as volatile CF<sub>4</sub>.

The XRD patterns of the as prepared MXene and the fluorinated MXene powders, for different time durations, are shown in Figure 1. The XRD pattern of the as prepared MXene in Figure 1a, is typical of an exfoliated Ti<sub>3</sub>AlC<sub>2</sub> pattern.<sup>1, 27</sup> It is evident that there are residual traces of Ti<sub>3</sub>AlC<sub>2</sub> after the HF solution treatment, indicating that not all the Ti<sub>3</sub>AlC<sub>2</sub> reacted with HF according to equation 1 during the 24 hour immersion period. In addition, weak TiO<sub>2</sub> peaks were observed in this pattern, which do not change during F<sub>2</sub> anneal. We note that the partial fluorination of trace TiO<sub>2</sub> impurity in the starting powder would have a minimal overall effect of the mass gain observed, and that in fact the 150 °C temperature is too low to effect full conversion to TiOF<sub>2</sub><sup>17</sup>. The weak, sharp peaks at 2θ ≈ 9.7° and 19.4° are the (002) and (004) reflections, respectively, from the Ti<sub>3</sub>AlC<sub>2</sub> phase. The broader peaks at slightly lower angles of 2θ ≈ 8.8° and 18.7° are from the newly formed MXene phase, indicating an expansion along the [0001] direction from a greater interlayer spacing. This occurs upon the loss of metallic bonding between in the presence of Al atoms, followed by OH<sup>-</sup> and F<sup>-</sup> surface functionalization, leading to the formation of smaller crystalline domains<sup>1</sup>. Fluorination of the MXene leads to mixed phase powders after 3 and 6 hours (see Figure 1b-c). After 3 hours of fluorination (FMX3) there is fluorination of the MXene surfaces, and peaks that can be indexed to the TiOF<sub>2</sub> phase start to emerge in the FMX3 pattern. With a longer fluorination time of 6 hours (FMX6) the peak intensity at 2θ ≈ 8.7° decreases, indicating a diminishing MXene phase content relative to TiOF<sub>2</sub>. By extending the fluorination time to 24 hours (FMX24) nearly single TiOF<sub>2</sub> phase is obtained (see Figure 1d); weak peaks from unreacted Ti<sub>3</sub>AlC<sub>2</sub> indicate that this compound is

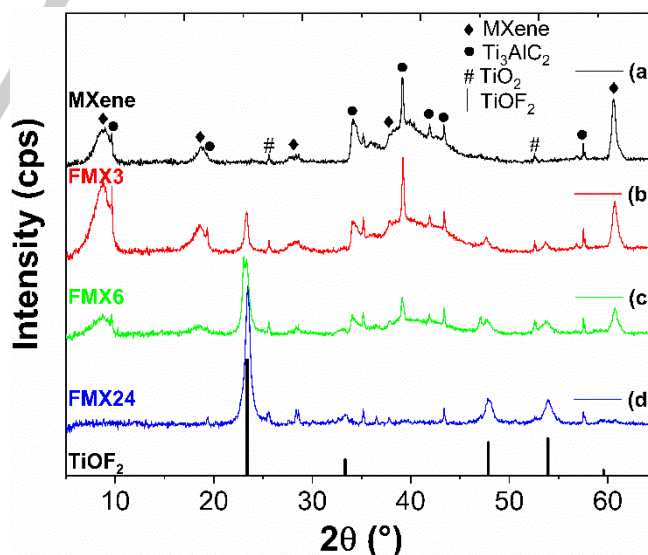


**Figure 1.** The XRD patterns of (a) the as prepared MXene powder (MXene), (b) the MXene powder fluorinated for 3 hours (FMX3), (c) the MXene powder fluorinated for 6 hours (FMX6) and (d) the MXene powder fluorinated for 24 hours (FMX24).

relatively inert to fluorine at 150 °C. The formation of a minute amount of  $\text{TiOF}_2$  in MXene samples was observed after heat treatment at 200 °C in Ar or  $\text{O}_2$  atmosphere by Li et al.<sup>27</sup> and reported to form from a low temperature reaction between  $\text{Ti}_3\text{C}_2$  with F termination and the O from ambient conditions or O/OH termination. A micrograph from the heat treated MXene powder (in  $\text{O}_2$  atmosphere) is reported to show  $\text{TiO}_2$  anatase nanocrystals that are distributed over the MXene sheets. However, with the use of  $\text{F}_2$ ,  $\text{TiOF}_2$  is gradually synthesized with an increase in the fluorination time. The SEM images of the as formed MXene and the fluorinated MXene are shown in Figure 2 where there is evidence for a sheet-like morphology in all samples. Single layers, that are less than 1 nm in thickness for the as prepared MXene powder, and become thicker on average with  $\text{F}_2$  annealing to ~150 nm per layer, as shown for FMX24 in Figure 2d. The thicknesses of the layers were approximated from the SEM images seen in Figure 2. Analysis of the FMX24 XRD data with the Scherrer equation estimates for the  $\text{TiOF}_2$  phase a crystalline domain size of approximately 16 nm, as compared to 5 nm for the starting MXene powder along the stacking direction [the (002) peak was used]. The fluorination produces some sintering and crystallization, but with overall retention of 2D particle morphology.

XPS was used to study the elemental composition of the C, Ti and F as a function of fluorination times on the surface of the MXene, FMX3, FMX6 and FMX24 particles. The surface content and ratios are shown in Table 2 and discussed in light of the fluorination time. The survey scans indicate the presence of Ti, C, O, F, Al and trace amounts (< 1 at.%) of N and S in the samples. It is shown in Table 2 that the surface elemental compositions of MXene, FMX3, FMX6 and FMX24 samples differ. Similar Ti/C ratios are observed for MXene and FMX6 (~0.35), which have the lowest capacity, and for FMX3 and FMX24 (~0.13) which have the highest capacity (increasing by an average of 77%). A similar trend with Ti/O is observed, with higher ratios for MXene and FMX6 (0.89 and 0.54), and lower for FMX3 and FMX24 (0.40 and 0.44).

However, the F content increases with fluorination time as expected, as indicated by an increasing F/Ti ratio from 0.38 to 3.66. The F/Ti ratios in the FMX6 and FMX24 samples are higher than expected for  $\text{TiOF}_2$  (a ratio of 0.5), suggesting excess F that is bound to carbon. The inconsistent trend in C and O content may reflect how inhomogeneities in the distribution of amorphous carbonaceous content affects the analysis, whereas the relative F content naturally increases with fluorination time.

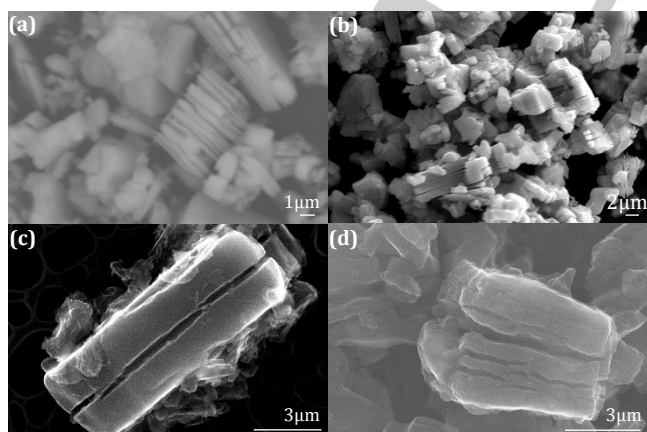


**Figure 2.** SEM images of (a) the as exfoliated  $\text{Ti}_3\text{C}_2$  and the fluorinated  $\text{Ti}_3\text{C}_2$  for (b) 3 hours (FMX3), (c) 6 hours (FMX6) and (d) 24 hours (FMX24).

**Table 2.** XPS measured elemental composition from survey scans of the MXene and its fluorinated counterpart samples showing the atomic concentrations of the elements.

Sample	Element [at.%]					Ratio		
	Ti	C	O	F	Al	Ti/O	Ti/C	F/Ti
MXene	17.5	51.5	19.6	6.6	4.5	0.9	0.3	0.4
FMX3	7.3	56.0	18.2	14.8	3.6	0.4	0.1	2.0
FMX6	11.2	30.8	20.7	32.2	5.1	0.5	0.4	2.9
FMX24	6.8	50.8	15.4	24.9	2.0	0.4	0.1	3.7

The high resolution XPS spectra of the C 1s, Ti 2p and F 1s core levels from MXene, FMX3, FMX6 and FMX24 are shown in Figure 3, which reveal information about the oxidation states and bonding at the surfaces. The C 1s spectra in Figure 3a show a peak corresponding to the C-C / C-H bonds at a binding energy (BE) of 284.8 eV. This peak is also used for charge correction for all the spectra. In addition to this peak, the presence of ether (C-OH, C-O-C) and ester (O-C=O) carbons, are also seen at BEs of 286.4 eV and ~289 eV, respectively. A peak at the lower BE of 281.9 eV that is related to the Ti-C bonds<sup>28, 29</sup> is seen for only MXene and FMX3. This indicates that the MXene phase is diminishing with fluorination and not observed on the surface of the FMX6 and FMX24 samples. High BE peaks (290.3 eV < BE < 291.8 eV) are visible for FMX3, FMX6 and FMX24 that corresponds to -C-F- bonds<sup>30</sup>, which are obviously due to the fluorination process that increases surface  $\text{F}_2$ . The -C-F- peak at the lower BE, is specifically related to  $\text{CF}_2$  groups (290.3 eV), as compared to the peaks at the higher BE that are related to  $\text{CF}_3$  groups<sup>31</sup>. After 6 hours of fluorination there is no sign of Ti-C bonds indicating that MXene is absent from the surface.  $\text{CF}_2$  groups are specifically seen on the FMX3 and FMX24 samples, which have superior electrochemical performance as compared to MXene and FMX6.

The Ti spectra indicate complex, sample dependent surface chemistry both in terms of oxidation state and bonding that results in electrodes having different electrochemical properties. The Ti 2p spectra in Figure 3b consists of a doublet (Ti 2p<sub>3/2</sub> and Ti 2p<sub>1/2</sub>) with a fixed doublet BE separation of 5.6 eV. The MXene and FMX3 have Ti 2p<sub>3/2</sub> peaks related to Ti-C bonds at a BE of 455.0 eV. The Ti 2p spectra of these two samples also have Ti peaks indicating the oxidation states 2+, 3+ and 4+ at BEs of ~456.3 eV, ~457.6 eV and ~459.2 eV, respectively. These Ti oxidation states are typically found in MXene materials<sup>32, 33</sup>. The spectrum of FMX3 contains an additional peak shifted towards higher BE at 460.8 eV that is related to fluorinated Ti<sup>3+</sup>. This relatively high BE peak can also be argued to be specifically related to  $\text{TiF}_3$ , which is electrochemically active<sup>35-37</sup>. The FMX6 and FMX24 samples show Ti spectra containing peaks from only  $\text{Ti}^{4+}$ , which was shown to be from the compound  $\text{TiOF}_2$ <sup>17, 38</sup>. The Ti spectra confirms the absence of Ti-C bonds in FMX6 and FMX24 and shows the formation of  $\text{TiOF}_2$  on these samples. It is also shown that  $\text{TiF}_3$  forms when MXene is fluorinated for 3 hours.

The spectra from F show the packing of F on the surface of the sheets and the confirmation of F bonds related to  $\text{TiOF}_2$ . The XPS spectra for F 1s are shown in Figure 3c where MXene and FMX6 show contributions from three peaks attributed to Ti-O-F bonds and two F-C peaks ( $F_{\text{LD-C}}$  and  $F_{\text{HD-C}}$ ) at BEs of 685.1 eV, ~687 eV and ~688 eV, respectively<sup>17, 39, 40</sup>. The peaks,  $F_{\text{LD-C}}$  and  $F_{\text{HD-C}}$  (in Figure 3c) corresponds to surface F at different densities. These peaks,  $F_{\text{LD-C}}$  and  $F_{\text{HD-C}}$  are attributed to the low- and high-density F coverage, respectively. It has also been reported that these peaks are attributed to semi-ionic ( $F_{\text{LD-C}}$ ) and covalent ( $F_{\text{HD-C}}$ ) C-F bonding<sup>41</sup>. An additional peak is found in the FMX3 spectrum at a higher BE of 689.4 eV attributed to  $\text{CF}_2$  as is also seen from the C 1s spectrum (see Figure 3a)<sup>42</sup>. The spectrum from the FMX24 sample shows only 2 peaks that are related to

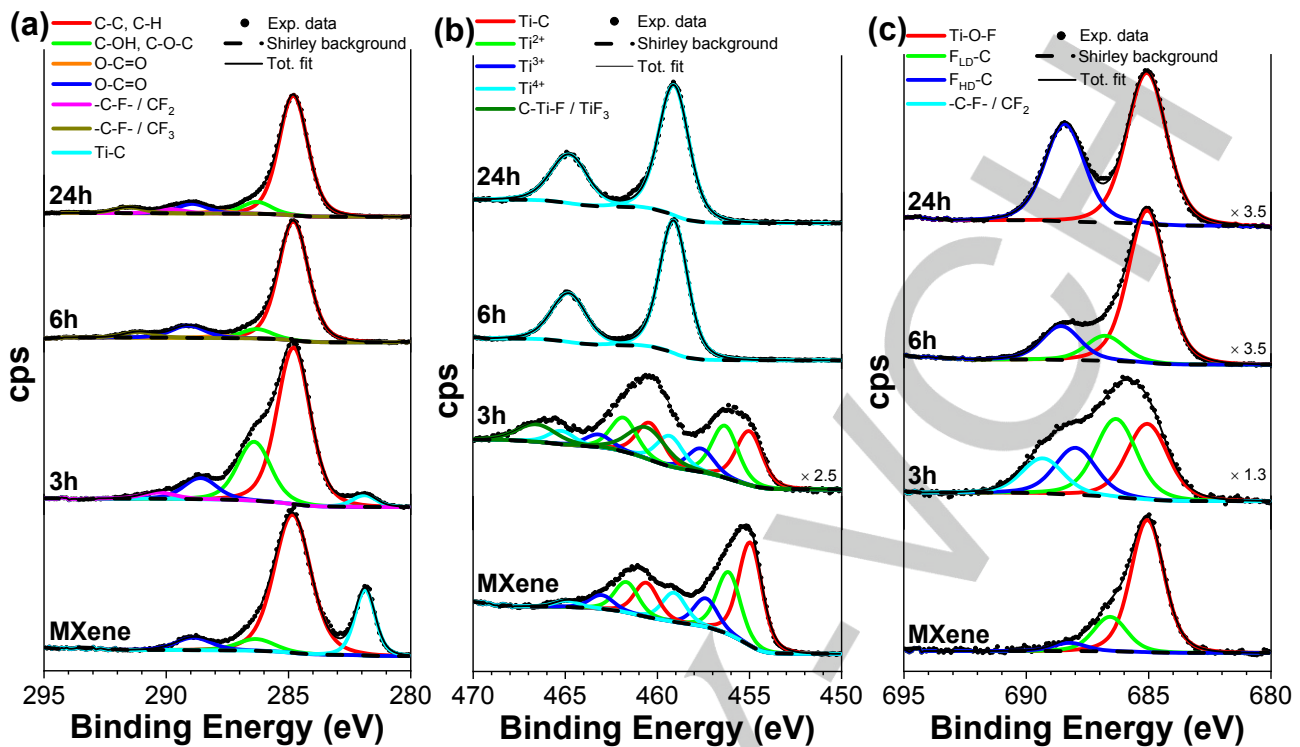


**Figure 3.** The XPS spectra of (a) the C 1s, (b) the Ti 2p and (c) the F 1s spectra from MXene and its fluorinated counterparts.

Ti-O-F bonds and covalently bonded F with a high surface coverage.

With higher fluorination times it is confirmed that the samples start to be dominated by two types of F, the Ti-O-F bond and densely packed covalently bonded F (F<sub>HD</sub>-C).

The fluorination mechanism of graphene (and related graphitic carbons) has been reported, as well as that of HF treated Ti<sub>3</sub>AlC<sub>2</sub>.<sup>1, 24, 41, 43, 44</sup> However, the direct fluorination (by elemental F<sub>2</sub>) mechanism of MXene has not been studied before. When MXene gets bombarded with F<sub>2</sub>, there is chemisorption of F onto the carbon surfaces and intercalation of the F between the layers. The nature of the F-C bond is dependent on the concentration of the F.<sup>45</sup> It is therefore observed from the F 1s XPS spectra (Figure 3c) that the HF treated Ti<sub>3</sub>AlC<sub>2</sub> (MXene) contains a high concentration F<sub>LD</sub>-C, that has a semi-ionic bond, and with an increase in the fluorination time the F<sub>LD</sub>-C concentration decreases and the F<sub>HD</sub>-C, containing a covalent bond, increases with no observable F<sub>LD</sub>-C peak after 24 hours fluorination (FMX24). The fluorination process of carbon transpires at the sp<sup>3</sup> C sites of the MXene where the oxygen containing groups are substituted by F atoms. More specifically, after 3 hours of fluorination CF<sub>2</sub> is observed that is reported to form by F<sup>-</sup> reacting with the carbonyl (-C=O) and epoxy (-C-O) groups<sup>31</sup> and when F substitutes COOH and OH groups semi-ionic and covalent C-F bonds are formed, respectively. Fluorinating the sample for 6 and 24 hours resulted in CF<sub>3</sub> to form on the surface of the material, with the XPS spectra (Figure 3c) predominantly showing F<sub>HD</sub>-C peaks. It is also possible that a significant amount of C does not form CF<sub>4</sub> and sublimates, with an increase in the F concentration, due to the weight gain of the samples observed in Table 1. A series of different possible reactions that can occur with the Ti from the Ti<sub>3</sub>C<sub>2</sub> and Ti<sub>3</sub>C<sub>2</sub>X<sub>2</sub> (X = OH, F) are shown as equations 3 – 4 for the product species observed. Specifically, with the MXene

having multiple Ti oxidation states (2+,3+ and 4+), the Ti<sup>3+</sup> compounds TiF<sub>3</sub> and TiOF<sub>2</sub> may readily start forming after 3 hours as seen from Figure 3b according to equation 7 – 10. After 6 hours of fluorination, given that TiF<sub>3</sub> is not observed in the XRD patterns (Figure 1), we may expect that much of the TiF<sub>3</sub> is converted to TiF<sub>4</sub> ( $TiF_3 + \frac{1}{2}F_2 \rightarrow TiF_4$ ) that can sublime away. With oxygen present TiOF<sub>2</sub> forms, becoming the dominant species on the surface for samples FMX6 and FMX24 as exemplified by the XRD and XPS results in Figure 1 and 3<sup>17, 46</sup>. It is evident from the micrographs in Figure 2 that MXene consists of exfoliated layers and that after fluorination these layers do not collapse. This can be explained by the strong C-F bond formation and the highly electronegative fluorine that causes a repulsion between the layers. This makes it possible to form layers with a TiOF<sub>2</sub> phase as seen from the XRD results in Figure 1. The excess F reacts with the remaining bulk C to form CF<sub>2</sub> in the FMX24 as seen from the C 1s XPS spectrum (see Figure 3a, top).

The electrochemical properties of MXene and its fluorinated counterparts, the FMX3, FMX6 and FMX24 materials as electrodes were examined using Li-ion half-cell batteries. These materials have different electrochemical properties. The cyclic voltammetry (CV) profiles, between 0.05 V and 3.0 V, in Figure 4a are in general pseudo-rectangular with redox peaks indicating a combination of diffusional (intercalation) and non-diffusional (capacitive) ion storage mechanism for these materials (see Figure S2). The two different current (*i*) contributions can be quantified for specific voltages (*V*) through  $i(V) = k_1v + k_2\sqrt{v}$ , where  $k_1v$  is the capacitive and  $k_2\sqrt{v}$  the intercalation contributions, with  $k_1$  and  $k_2$  being constants and  $v$  the scan rate<sup>47</sup>. The calculation is discussed in the supplementary information and figure S2b. Figure S3 show the capacitance contributions of

the four electrodes as 17%, 27%, 7% and 14% for MXene, FMX3, FMX6 and FMX24, respectively. The MXene shows two reversible peaks with anodic / cathodic peak values of  $\sim 0.9$  V /  $\sim 0.8$  V and  $\sim 2.4$  V /  $\sim 2.2$  V which is similar to other  $\text{Ti}_3\text{C}_2$  materials reported<sup>48</sup>. The FMX3 profile shows more peaks, which is the result of the electrochemically active  $\text{TiF}_3$  present, as observed from the XPS results (see Figure 3b). In the anodic and cathodic sweeps anodic / cathodic peaks are found at  $\sim 1.0$  V /  $\sim 0.9$  V and  $\sim 2.5$  V /  $\sim 2.4$  V which are consistent with MXene and at  $\sim 1.5$  V /  $\sim 1.1$  V,  $\sim 1.9$  V /  $\sim 1.6$  V and  $\sim 2.2$  V /  $\sim 2.2$  V which are consistent with the discharge and charge profiles of  $\text{TiF}_3$ <sup>36</sup>. FMX6 having a broad anodic peak around  $\sim 1.1$  V and a less broad peak at 2.1 V which could be related to the charge process of MXene. In the cathodic sweep there is no obvious indication of a peak at the higher potentials, as would be expected for MXene. However, a broad peak at  $\sim 1.1$  V and a sharp peak at  $\sim 0.9$  V are observed, with the sharp peak broadening with an increase in sweep rate (see Figure S1). This indicates that FMX6 does not have a good rate capability. FMX24 is more pseudo-rectangular with broad anodic / cathodic peaks around  $\sim 1.2$  V /  $\sim 0.9$  V. These peaks are consistent with the reported discharge / charge profiles for  $\text{TiO}_2$  fluorinated to form  $\text{TiOF}_2$ <sup>17</sup>. With MXene, FMX3 and FMX6 having semi-ionic C-F bonds (see figure 3c) the anodic / cathodic peaks at  $\sim 1.1$  V /  $\sim 0.9$  V could be as a result of these bonds converting to ionic bonds, reversibly, by interacting with Li. It was reported that during the discharge process with the translation of C-F bonds from semi-ionic to ionic the F ions are bonded to Li ions through electrostatic interactions. During the charge process the F ions are close to the carbocation and thus will reconstruct the semi-ionic C-F bonds<sup>11</sup>. The CV shows that MXene, when fluorinated have different electrochemical properties. In fact, the FMX3 sample shows the electrochemical signatures of  $\text{TiF}_3$  as was shown to be present by means of XPS. The FMX24 shows typical electrochemical properties related to  $\text{TiOF}_2$ , confirming the XRD and XPS results.

The charge/discharge profiles were examined to show the differences of the fluorinated MXene to that of the as synthesized MXene and also for differences from prior work, which may reflect the influence of the plate-like particle morphology. Figure 4b-c show the initial, 2<sup>nd</sup> and 50<sup>th</sup> discharge profiles of MXene and its

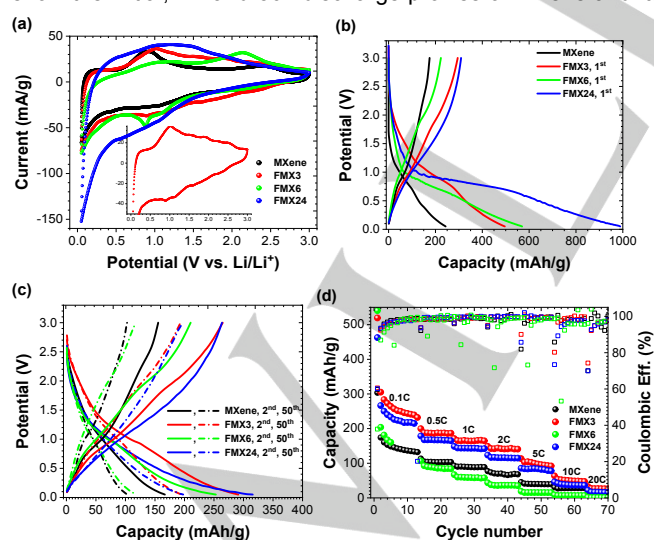


**Figure 4.** A comparison of the MXene, FMX3, FMX6 and FMX24 by (a) cyclic voltammetry at a sweep rate of 0.1 mV/s, (b) initial discharge profiles discharged at 0.1C, (c) 2<sup>nd</sup> and 50<sup>th</sup> discharge profiles at 1C and (d) rate capability.

fluorinated counterparts. The initial discharge profile of MXene shows no obvious plateau with a relatively small initial irreversible capacity loss of 31.3 % as expected from the low surface area ( $9 \text{ m}^2/\text{g}$ ). Thus the majority of the capacity loss is from the irreversible reduction of electrochemically active surface groups<sup>49</sup>. The initial capacity loss from the MXene is considerably less compared to the 41.3 %, 55.6 % and 68.0 % from the fluorinated FMX3, FMX6 and FMX24, respectively. The increase in the initial capacity loss cannot be justified by the minute increases in surface areas, which are  $9 \text{ m}^2/\text{g}$ ,  $12 \text{ m}^2/\text{g}$  and  $14 \text{ m}^2/\text{g}$  for FMX3, FMX6 and FMX24, respectively. Therefore, the plateau observed in figure 4b for FMX3, is not due to SEI formation, but rather from the reversible reactions from  $\text{TiF}_3$ , as is also seen in the subsequent cycles in figure 4c. It is expected, that with increased fluorination time more surface F would be present (with the exception of FMX24), as seen from Table 2, which is known to reduce irreversibly<sup>42,49</sup>. The capacity loss for FMX6 is thus from F surface groups that reduced irreversibly during the first discharge. A plateau at  $\sim 0.9$  V in the 2<sup>nd</sup> discharge profile of FMX6 is consistent with discharge profiles of  $\text{TiOF}_2$ , which is evidenced in the XRD data (see figure 1c). In the XRD results, the  $\text{TiOF}_2$  (see figure 1d) is much more prominent in the FMX24 sample and thus the plateau at  $\sim 0.9$  V is the result of an amorphization process<sup>16,17</sup>. The 2<sup>nd</sup> discharge profile of the FMX24 is similar to that of FMX6 confirming it coming from the  $\text{TiOF}_2$ . In the 50<sup>th</sup> discharge profiles the plateau  $\sim 0.9$  V is still prominent for all the samples. It is seen from the XPS results (see figure 3b) that the semi-ionic C-F bonds increase, in order, for FMX3, MXene and FMX6. Therefore, the  $\sim 0.9$  V plateau for these materials are considered to be from the C-F bonds transformation, from semi-ionic to ionic and vice versa, in addition to the  $\text{TiF}_3$  based reactions for the FMX3. The  $\sim 0.9$  V plateau from the FMX24 is intrinsic from  $\text{TiOF}_2$ <sup>16</sup>.

Figure 4d shows the rate capability of the materials where FMX3 and FMX24 show the best rate performance with FMX3 being the best. MXene and FMX6 are inferior to the latter two samples with MXene being superior compared to FMX6. With an increase of the current by a factor of 10 (0.1C to 1C;  $0.026 \text{ A/g}$  to  $0.26 \text{ A/g}$ ) MXene, FMX3, FMX6 and FMX24 lose approximately 38 %, 35 %, 63 % and 36 %, respectively, of their initial stable capacity. The FMX24 sample having mainly a  $\text{TiOF}_2$  phase with a 2D sheet like morphology is superior to the  $\text{TiOF}_2$  formed from fluorinating  $\text{TiO}_2$ . The  $\text{TiOF}_2$  formed from  $\text{TiO}_2$  loses more than 70 % of its initial stable capacity by increasing the current by a factor of ten<sup>17</sup>. The superior rate capability of the  $\text{TiOF}_2$  formed from MXene can be ascribed to the 2D layered morphological structure that would result in a reduced drag for Li diffusion.

The direct fluorination time of MXene, the different Ti and F species and its content affects both the capacity and its retention and rate capability. The capacity retention at a 0.1C ( $0.1\text{C} = 0.026 \text{ A/g}$ ), as seen in Figure 5a, the capacity loss over typically the first 10 is the highest due to the irreversible reduction of the surface functional groups. The capacity loss over this range is 24.6 %, 22.3 %, 45.1 % and 34.5 % for MXene, FMX3, FMX6 and FMX24, respectively. This is consistent with the surface F content on each sample (Table 2), taking into account that FMX3 has formed  $\text{TiF}_3$  and FMX24  $\text{TiOF}_2$ . The capacity loss from the 10<sup>th</sup> to the 120<sup>th</sup> cycle is 18.3 %, 17.3 % and 10.8 % for MXene, FMX3 and FM6, respectively. However, the FMX24 sample shows an increase of 13.0 % in the capacity from the 10<sup>th</sup> to the 120<sup>th</sup> cycle. A similar trend is observed when cycled at a higher c-rate of 1C ( $0.26 \text{ A/g}$ ), in Figure 5b, with the exception of FMX6 having the least capacity performance. It is evident that FMX3 and FMX24 have superior electrochemical performance. It is worth noting that these two materials have a similar CF<sub>2</sub> groups on Li on the surface (see Figure 3b).

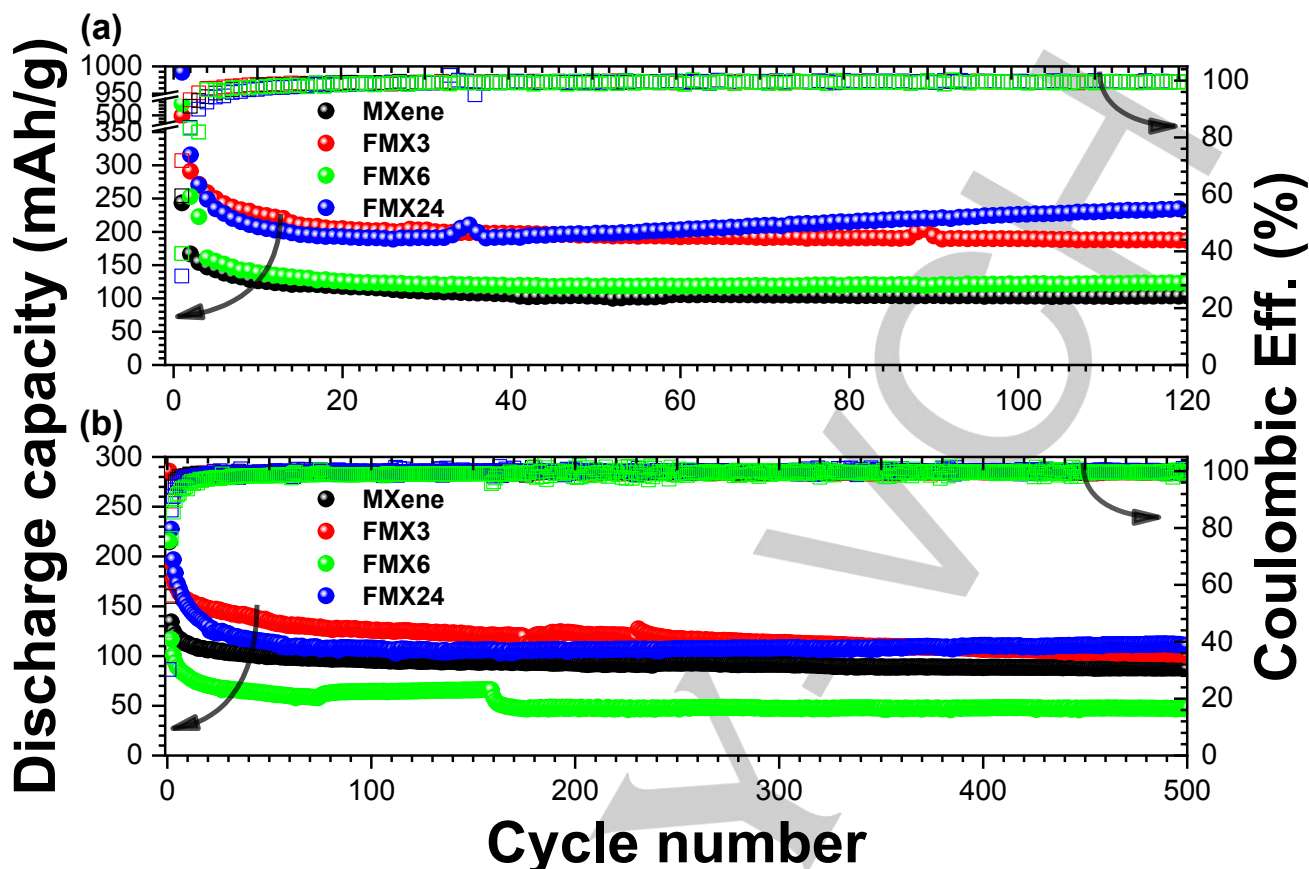


**Figure 5.** Discharge capacities and coulombic efficiencies for extended cycling (a) at 0.1C for 120 cycles and (b) at 1C for 500 cycles.

It has been shown that  $\text{CF}_2$  doped graphene oxide have superior electrochemical performance and cycling stability. This is due to the vacancies that accompany the formation of  $\text{CF}_2$  groups (on the FMX6 and FMX24) acting as active sites that enhances the  $\text{Li}^+$  storage capacity<sup>31</sup>. Also, the  $\text{TiF}_3$  and  $\text{CF}_2$  formed after 3 hours of fluorination, that is electrochemically active, on FMX3 is transformed to  $\text{TiF}_4$  and  $\text{CF}_3$ , respectively, after 6 hours of fluorination on FMX6 that sublimated and is electrochemically inactive, respectively. This causes a reduction in the capacity of FMX6. In addition to this we have also shown, in Figure S3, that the capacitance contribution decreases from 27% to 7% from FMX3 to FMX6. In the case for the  $\text{TiOF}_2$  it is noted that it intrinsically has a better electrochemical performance as compared to MXene<sup>18</sup>.

## Conclusions

Direct fluorination of  $\text{Ti}_3\text{C}_2\text{X}_2$  ( $\text{X} = \text{OH}, \text{O}, \text{F}$ ), synthesized from commercial  $\text{Ti}_3\text{AlC}_2$ , for 3h, 6h and 24, respectively, by means of a purpose-built fluidized bed reactor (FBR) for fluorination. The fluorinated samples changed from a MXene based phase to  $\text{TiOF}_2$ , with FMX24 having practically a pure phase. Despite the MXene changing to a different phase, with fluorination, it retained the 2D layered morphology. The 24h fluorinated sample (FMX24) thus have a  $\text{TiOF}_2$  phase with a 2D layered morphology that

facilitates ion diffusion. When MXene is fluorinated for 3h (FMX3)  $\text{TiF}_3$  is formed which are electrochemically active. Also,  $\text{CF}_2$  groups are evident on the surfaces of FMX3 and FMX24 that are electrochemically beneficial during the charge / discharge process. In addition, FMX3 and FMX24, that have the best electrochemical performance, have a similar Ti/C ratio. All the fluorinated materials have cycling stabilities superior to MXene, which already has a good cycling stability. FMX24 with its  $\text{TiOF}_2$  phase has good capacity with an increasing capacity with cycle number. FMX24 has a better rate capability as compared to a non 2D layered  $\text{TiOF}_2$ , indicating the advantage of the 2D layered morphology.

## Experimental Section

**Material synthesis.**  $\text{Ti}_3\text{C}_2\text{X}_2$  ( $\text{X} = \text{OH}, \text{O}, \text{F}$ ) was synthesized from  $\text{Ti}_3\text{AlC}_2$  where the Al atoms were removed by means of HF etching, as has been reported<sup>49</sup>. Typically, 10 g of commercial  $\text{Ti}_3\text{AlC}_2$  powders were added into a 49 wt. % HF solution, heated to 60 °C and continuously stirred for 24 hours. The suspension was further centrifuged and thoroughly rinsed with deionized water up to a solution pH of > 6. The product was finally washed with ethanol and then

dried at 60 °C for 24 h and here forth denoted as MXene. The fluorination of MXene powders were carried out in a fluidized bed reactor (FBR) setup as shown in Figure 6. Before the fluorination process, MXene powders were dried at 150 °C under high vacuum overnight in order to remove “free” water. The FBR is connected to a gas mixing device with a flow transducer for F<sub>2</sub> gas and a rotameter gauge flowmeter for the N<sub>2</sub> gas. The F<sub>2</sub> gas used in this experiment is 20 % F<sub>2</sub> in N<sub>2</sub>. The dehydrated MXene was weighed and placed in the FBR tube and hermitically sealed. Before ramping the temperature, the FBR tube containing the MXene powder

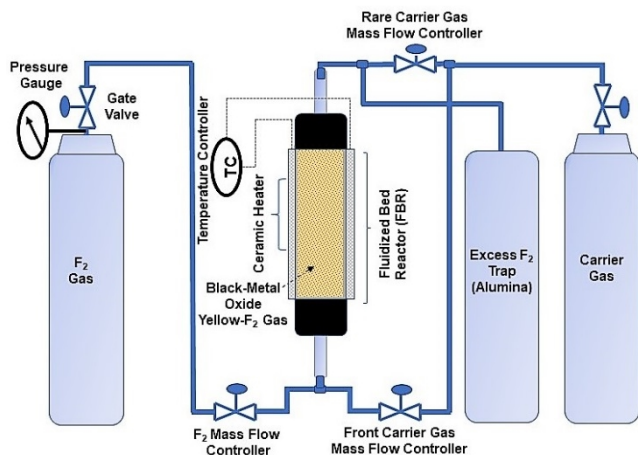


**Figure 6.** Diagram of the fluidized bed reactor (FBR) setup used for the fluorination.

was purged for 1 hour with flowing N<sub>2</sub> gas. The FBR tube temperature was then increased to 130 °C (or 150 °C), and once the temperature was reached, F<sub>2</sub> gas was allowed to pass through the FBR tube along with N<sub>2</sub> gas as the carrier gas supply.

After the predetermined fluorination time (see Table 1), F<sub>2</sub> gas flow was stopped and the FBR tube was allowed to cool to room temperature under N<sub>2</sub> gas flow. Once the FBR tube was at room temperature it was detached from the reactor system. The fluorinated MXene samples, denoted here forth as FMX3, FMX6 and FMX24 for 3, 6 and 24 hours of fluorination, respectively, were weighed before and after fluorination to determine the weight gain as shown in Table 1. The experimental conditions used are summarized in Table 1.

**Chemical and microstructural characterization.** The X-ray diffraction (XRD) patterns were collected on a Panalytical Empyriam X-ray diffractometer using Cu K<sub>α</sub> radiation at 40 kV and 20 mA over a 2θ range from 5° to 65°, counting for 150s per step of 0.026°. Micrographs of the samples were obtained from a Zeiss EVO-MA15 scanning electron microscope (SEM). The X-ray photoelectron spectroscopy (XPS) data were obtained using a Thermo Scientific (Waltham, MA, USA) Model K-Alpha instrument, with a

monochromated, micro-focusing Al K<sub>α</sub> X-ray source (1486.6 eV).

**Electrochemical characterization.** Electrodes of MXene, FMX3, FMX6 and FMX24 were prepared by mixing the active material with carbon black and polyvinylidene fluoride (PVDF) binder in N-methyl-2-pyrrolidinone (NMP), with a weight ratio of 8:1:1, to form a slurry. The slurry mixtures were cast on a copper foil and dried at 80 °C in high vacuum overnight. The electrodes were transferred to an argon-filled glove box, and coin cells were assembled using Li foil as counter and reference electrode, Celgard as an insulating microporous separator, and the MXene, FMX3, FMX6 or FMX24 as a working electrode. A 1 M LiPF<sub>6</sub> in a mixture of ethylene carbonate (EC) / ethylmethyl carbonate (EMC) / dimethyl carbonate (DMC), in a 1:1:1 volume ratio, were used as the electrolyte. Coin cells were cycled between 0.05 and 3.0 V versus Li<sup>+</sup>/Li at different current densities (with 1C = 260 mA/g) with an Arbin instrument. Cyclic voltammetry (CV) was performed on a Biologic VSP instrument in the voltage range 0.05 V – 3.0 V.

## Acknowledgements

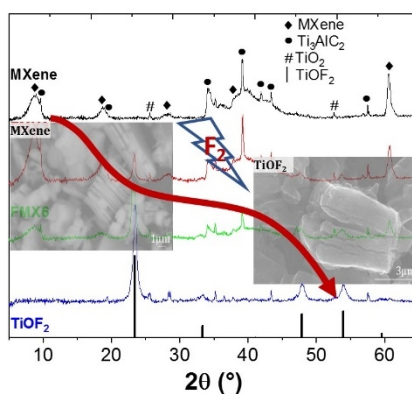
This work was supported by the U.S. Department of Energy, Office of Science, Basic Energy Sciences, Materials Sciences and Engineering Division.

**Keywords:** MXene • Fluorination • Elemental F<sub>2</sub> • TiOF<sub>2</sub> • Lithium-ion batteries

- [1] M. Naguib, M. Kurtoglu, V. Presser, J. Lu, J. Niu, M. Heon, L. Hultman, Y. Gogotsi, M. W. Barsoum *Adv Mater.* 2011, 23, 4248-4253.
- [2] A. Feng, Y. Yu, Y. Wang, F. Jiang, Y. Yu, L. Mi, L. Song *Materials & Design.* 2017, 114, 161-166.
- [3] M. Ghidui, M. R. Lukatskaya, M. Q. Zhao, Y. Gogotsi, M. W. Barsoum *Nature.* 2014, 516, 78-81.
- [4] J. Pang, R. G. Mendes, A. Bachmatiuk, L. Zhao, H. Q. Ta, T. Gemming, H. Liu, Z. Liu, M. H. Rummeli *Chem Soc Rev.* 2019, 48, 72-133.
- [5] M. Okubo, A. Sugahara, S. Kajiyama, A. Yamada *Acc Chem Res.* 2018, 51, 591-599.
- [6] J. Luo, X. Tao, J. Zhang, Y. Xia, H. Huang, L. Zhang, Y. Gan, C. Liang, W. Zhang *ACS Nano.* 2016, 10, 2491-2499.
- [7] J. Luo, W. Zhang, H. Yuan, C. Jin, L. Zhang, H. Huang, C. Liang, Y. Xia, J. Zhang, Y. Gan, X. Tao *ACS Nano.* 2017, 11, 2459-2469.
- [8] J. Luo, C. Wang, H. Wang, X. Hu, E. Matios, X. Lu, W. Zhang, X. Tao, W. Li *Advanced Functional Materials.* 2019, 29.
- [9] H. Zhang, X. Xin, H. Liu, H. Huang, N. Chen, Y. Xie, W. Deng, C. Guo, W. Yang *The Journal of Physical Chemistry C.* 2019.
- [10] R. Cheng, T. Hu, H. Zhang, C. Wang, M. Hu, J. Yang, C. Cui, T. Guang, C. Li, C. Shi, P. Hou, X. Wang *The Journal of Physical Chemistry C.* 2018, 123, 1099-1109.
- [11] J. He, N. Wang, Z. Yang, X. Shen, K. Wang, C. Huang, Y. Yi, Z. Tu, Y. Li *Energy & Environmental Science.* 2018, 11, 2893-2903.
- [12] Z. Ma, X. Zhou, W. Deng, D. Lei, Z. Liu *ACS Appl Mater Interfaces.* 2018, 10, 3634-3643.
- [13] M. Khazaei, M. Arai, T. Sasaki, C.-Y. Chung, N. S. Venkataramanan, M. Estili, Y. Sakka, Y. Kawazoe *Advanced Functional Materials.* 2013, 23, 2185-2192.
- [14] R. B. Rakhi, B. Ahmed, M. N. Hedhili, D. H. Anjum, H. N. Alshareef *Chemistry of Materials.* 2015, 27, 5314-5323.
- [15] S.-T. Myung, M. Kikuchi, C. S. Yoon, H. Yashiro, Y.-K. Sun *Journal of Power Sources.* 2015, 288, 376-383.
- [16] M. V. Reddy, S. Madhavi, G. V. Subba Rao, B. V. R. Chowdari *Journal of Power Sources.* 2006, 162, 1312-1321.

- [17] J. M. Powell, J. Adcock, S. Dai, G. M. Veith, C. A. Bridges RSC Advances. 2015, 5, 88876-88885.
- [18] D. Deng ChemNanoMat. 2017, 3, 146-159.
- [19] R. R. Nair, W. Ren, R. Jalil, I. Riaz, V. G. Kravets, L. Britnell, P. Blake, F. Schedin, A. S. Mayorov, S. Yuan, M. I. Katsnelson, H. M. Cheng, W. Strupinski, L. G. Bulusheva, A. V. Okotrub, I. V. Grigorieva, A. N. Grigorenko, K. S. Novoselov, A. K. Geim Small. 2010, 6, 2877-2884.
- [20] P. F. Fulvio, S. S. Brown, J. Adcock, R. T. Mayes, B. Guo, X.-G. Sun, S. M. Mahurin, G. M. Veith, S. Dai Chemistry of Materials. 2011, 23, 4420-4427.
- [21] J. Xiao, P. Meduri, H. Chen, Z. Wang, F. Gao, J. Hu, J. Feng, M. Hu, S. Dai, S. Brown, J. L. Adcock, Z. Deng, J. Liu, G. L. Graff, I. A. Aksay, J. G. Zhang ChemSusChem. 2014, 7, 1295-1300.
- [22] P. F. Fulvio, G. M. Veith, J. L. Adcock, S. S. Brown, R. T. Mayes, X. Wang, S. M. Mahurin, B. Guo, X.-G. Sun, A. A. Puretzky, C. M. Rouleau, D. B. Geohegan, S. Dai Journal of Materials Chemistry A. 2013, 1.
- [23] H. Zhou, R. E. Ruther, J. Adcock, W. Zhou, S. Dai, J. Nanda ACS Nano. 2015, 9, 2530-2539.
- [24] Z. Wang, J. Wang, Z. Li, P. Gong, X. Liu, L. Zhang, J. Ren, H. Wang, S. Yang Carbon. 2012, 50, 5403-5410.
- [25] J.-C. Lei, X. Zhang, Z. Zhou Frontiers of Physics. 2015, 10, 276-286.
- [26] Z. A. Qiao, S. S. Brown, J. Adcock, G. M. Veith, J. C. Bauer, E. A. Payzant, R. R. Unocic, S. Dai Angew Chem Int Ed Engl. 2012, 51, 2888-2893.
- [27] Z. Li, L. Wang, D. Sun, Y. Zhang, B. Liu, Q. Hu, A. Zhou Materials Science and Engineering: B. 2015, 191, 33-40.
- [28] E. H. Kisi, J. A. A. Crossley, S. Myhra, M. W. Barsoum Journal of Physics and Chemistry of Solids. 1998, 59, 1437-1443.
- [29] S. Myhra, J. A. A. Crossley, M. W. Barsoum Journal of Physics and Chemistry of Solids. 2001, 62, 811-817.
- [30] C. Struzzi, M. Scardamaglia, N. Reckinger, H. Sezen, M. Amati, L. Gregoratti, J. F. Colomer, C. Ewels, R. Snyders, C. Bittencourt Phys Chem Chem Phys. 2017, 19, 31418-31428.
- [31] H. An, Y. Li, Y. Feng, Y. Cao, C. Cao, P. Long, S. Li, W. Feng Chem Commun (Camb). 2018, 54, 2727-2730.
- [32] G. Liu, J. Shen, Q. Liu, G. Liu, J. Xiong, J. Yang, W. Jin Journal of Membrane Science. 2018, 548, 548-558.
- [33] C. Peng, H. Wang, H. Yu, F. Peng Materials Research Bulletin. 2017, 89, 16-25.
- [34] T. Sultana, G. L. Georgiev, G. Auner, G. Newaz, H. J. Herfurth, R. Patwa Applied Surface Science. 2008, 255, 2569-2573.
- [35] G. Ramanath, J. E. Greene, J. R. A. Carlsson, L. H. Allen, V. C. Hornback, D. J. Allman Journal of Applied Physics. 1999, 85, 1961-1969.
- [36] H. Li, G. Richter, J. Maier Advanced Materials. 2003, 15, 736-739.
- [37] I. Hotovy, S. Hascik, M. Gregor, V. Rehacek, M. Predanoc, A. Plecenik Vacuum. 2014, 107, 20-22.
- [38] C. Z. Wen, Q. H. Hu, Y. N. Guo, X. Q. Gong, S. Z. Qiao, H. G. Yang Chem Commun (Camb). 2011, 47, 6138-6140.
- [39] D. Li, H. Haneda, S. Hishita, N. Ohashi Chemistry of Materials. 2005, 17, 2588-2595.
- [40] M. Senna, V. Šepelák, J. Shi, B. Bauer, A. Feldhoff, V. Laporte, K.-D. Becker Journal of Solid State Chemistry. 2012, 187, 51-57.
- [41] S. Huang, Y. Li, Y. Feng, H. An, P. Long, C. Qin, W. Feng Journal of Materials Chemistry A. 2015, 3, 23095-23105.
- [42] P. Fan, H. Liu, L. Liao, Z. Wang, Y. Wu, Z. Zhang, Y. Hai, G. Lv, L. Mei Electrochimica Acta. 2018, 289, 407-414.
- [43] H. An, Y. Li, P. Long, Y. Gao, C. Qin, C. Cao, Y. Feng, W. Feng Journal of Power Sources. 2016, 312, 146-155.
- [44] O. Jankovský, P. Šimek, D. Sedmidubský, S. Matějková, Z. Janoušek, F. Šembera, M. Pumera, Z. Sofer RSC Adv. 2014, 4, 1378-1387.
- [45] S. Zhou, S. D. Sherpa, D. W. Hess, A. Bongiorno The Journal of Physical Chemistry C. 2014, 118, 26402-26408.
- [46] N. Batisse, K. Guérin, M. Dubois, A. Hamwi Carbon. 2011, 49, 2998-3009.
- [47] J. Luo, C. Fang, C. Jin, H. Yuan, O. Sheng, R. Fang, W. Zhang, H. Huang, Y. Gan, Y. Xia, C. Liang, J. Zhang, W. Li, X. Tao Journal of Materials Chemistry A. 2018, 6, 7794-7806.
- [48] F. Du, H. Tang, L. Pan, T. Zhang, H. Lu, J. Xiong, J. Yang, C. Zhang Electrochimica Acta. 2017, 235, 690-699.
- [49] M. Naguib, J. Come, B. Dyatkin, V. Presser, P.-L. Taberna, P. Simon, M. W. Barsoum, Y. Gogotsi Electrochemistry Communications. 2012, 16, 61-64.

The transformation of MXene 2D sheets into  $\text{TiOF}_2$  sheets with superior electrochemical performance. MXene fluorinated by means of a direct fluorination process for 24 hours is transformed to  $\text{TiOF}_2$ , maintaining the 2D layer morphology. This material exhibits increased capacity, high rate capability and long cycling stability.



*Bishnu P. Thapaliya, Charl J. Jafta,\*  
Hailong Lyu, Jiexiang Xia, Harry M.  
Meyer III, M. Parans Paranthaman,  
Xiao-Guang Sun, Craig A. Bridges, and  
Sheng Dai\**

**Page No. – Page No.**

**Fluorination of Mxene by Elemental  
 $\text{F}_2$  as Electrode Material for Lithium-  
Ion Batteries**